Structural and electronic properties of defects at grain boundaries in CuInSe$_2$

R. Saniz,[1] J. Bekaert,[1] B. Partoens,[1] and D. Lamoen[2]

[1]*CMT, Departement Fysica, Universiteit Antwerpen,*
Groenenborgerlaan 171, B-2020 Antwerpen, Belgium
[2]*EMAT, Departement Fysica, Universiteit Antwerpen,*
Groenenborgerlaan 171, B-2020 Antwerpen, Belgium

We report on a first-principles study of the structural and electronic properties of a $\Sigma 3$ (112) grain boundary model in CuInSe$_2$. The study focuses on a coherent, stoichiometry preserving, cation-Se terminated grain boundary, addressing the properties of the grain boundary as such, as well as the effect of well known defects in CuInSe$_2$. We show that in spite of its apparent simplicity, such a grain boundary exhibits a very rich phenomenology, providing an explanation for several of the experimentally observed properties of grain boundaries in CuInSe$_2$ thin films. In particular, we show that the combined effect of Cu vacancies and cation antisites can result in the observed Cu depletion with no In enrichment at the grain boundaries. Furthermore, Cu vacancies are unlikely to produce a hole barrier at the grain boundaries, but Na may indeed have such an effect. We find that Na-on-Cu defects will tend to form abundantly at the grain boundaries, and can provide a mechanism for the carrier depletion and/or type inversion experimentally reported.

PACS numbers:

I. INTRODUCTION

Currently, one of the leading thin-film photovoltaic (PV) cell technologies is based on absorber layers made of the chalcopyrite Cu(In,Ga)Se$_2$ (CIGS). Very recently, an efficiency of 22.6% has been achieved with a CIGS based PV cell, setting a new world record for the thin-film technologies[1] and outperforming multicrystalline silicon cells by 1.3% points.[2] This brings the CIGS based PV cells much closer to be a real alternative to the Si-based technologies that still dominate the market. The potential of the CIGS absorber layers was recognized early on. The continued interest they have elicited during the past several years is reflected in the considerable literature on research efforts aiming at a deeper understanding of their properties (see, e.g., Refs. 3–5, and references therein).

A striking aspect of the CIGS absorber layers is that the relatively high density of grain boundaries (GBs) they typically exhibit has not been found to be detrimental to the efficiency of the cells. What is more, the PV cells made with polycrystalline CIGS are significantly more efficient than those made with CIGS single crystals.[6] It is, thus, important to try to have a more detailed understanding of the effects of GBs on the electronic properties of the CIGS absorber layers; not only for fundamental reasons but also because such an understanding can help increase further the efficiency of the PV cells. This is the reason why in recent years many researchers have been performing measurements that focus specifically on the grain boundaries, trying to characterize them better and to determine the role they play in charge carrier recombination and transport.[6–12] In spite of the advances, several open questions remain today, and how exactly the GBs affect the efficiency of the PV cells is still under debate. From the theoretical point of view, the task is also difficult. GBs are complex systems, and rather challenging to model, especially using first-principles computational

methods. Nevertheless, the latter have contributed importantly to the debate in several respects, whether introducing a GB model in which electron-hole recombination is prevented,[13] discussing defect segregation to the GBs[14–17] or studying band edge shifts and gap states at the GBs.[18]

CIGS is obtained by alloying CuInSe$_2$ (CIS) with CuGaSe$_2$ (CGS). These have band gaps of ~ 1 eV and ~ 1.7 eV, respectively.[19] The purpose of the alloying is to tune the band gap of the alloy and thus optimize the efficiency of the PV cell. Because of the similarity between the structural and electronic properties of CIS and CGS,[3,20,21] it is expected that the study of these two compounds can shed light on the properties of the alloy. Thus, for simplicity, most theoretical reports in the literature focus either on CIS or CGS.[17,22–26] This is true for the GB studies mentioned as well. It has been experimentally determined that the most common GBs in these chalcopyrites are $\Sigma 3$ GBs.[6,27] Hence, several groups have reported investigations of $\Sigma 3$ GBs using first-principles methods.[14–16,18,29,30] However, often these works are based on the use of local or semi-local exchange-correlation potentials.[14–16,29] In general, these are sufficient to obtain reliable trends regarding structural changes in semiconductors, but it is known that they are not reliable enough to determine electronic properties such as band edge shifts, gap state energies, or the formation energy of defects and charge transition levels.[31] Furthermore, there are several classes or types of $\Sigma 3$ GBs that can occur in the chalcopyrites. For instance, these can be cation-Se, cation-cation, or Se-Se terminated,[11,12] and can occur along (112) planes or (114) planes.[10,12]

Here, we present a first-principles study of the structural and electronic properties of a (112), cation-Se terminated $\Sigma 3$ GB in CIS. Our study focuses in particular on the effect of defects. To determine the structural parameters of the systems considered, we use a semi-

local functional, as previous authors. But to determine the electronic properties and related quantities we use a hybrid functional approach. Compared to alternative approaches, such as those based on quasi-particle methods, it offers the best compromise between computational cost and accuracy when it comes to the study of the electronic structure of systems as large as the ones considered here.[31] Our work goes beyond previous first-principles studies of GBs,[18,30] looking in more detail into the interaction of defects and $\Sigma 3$ GBs, and calculating charged defect formation energies and their transition levels. The results shed new light on the complex effects that these GBs can have on the electronic properties of CIS absorbers layers.

In Section II we discuss in more detail the methods and model used in our work. In Section III we present and discuss our results. The last section presents a brief summary and the main conclusions of our work.

II. METHODOLOGY AND MODEL

A. Computational aspects

We performed all our first-principles calculations with the VASP code,[32] using the projector augmented wave method (PAW) to describe the electron-ion interactions.[33] The Cu $3d4s$, In $4d5s5p$, Se $4s4p$, and Na $3s$ electrons (which we study as an impurity) are treated as valence. The plane wave basis set energy cutoff was set to 500 eV, a value optimized in a previous work on native point defects in CIGS compounds.[26] Total energies were converged to within 10^{-5} eV. Geometry optimizations were done using the Perdew-Burke-Ernzerhof (PBE) exchange and correlation functional.[34] Forces were converged to within 0.02 eV/Å, using the VASP method based on the conjugate-gradient algorithm. In the case of charged defect calculations, as in most first-principles codes, a compensating homogeneous background charge density is introduced in order to ensure charge neutrality. Our CIS $\Sigma 3$ GB model consists of a supercell of 288 atoms (i.e., 72 formula units), as described in more detail further on. The dimensions of the optimized supercell are $14.26 \times 16.69 \times 30.77$ Å. We used a $2 \times 2 \times 1$ **k**-point mesh for all our GB calculations.

We note that previous studies of GBs in CIS were based on the PBE+U correction to PBE, essentially to try to improve the description of the electronic structure. Different U (or $U - J$) values have been used by different authors, but in all cases the band gap of CIS remains greatly underestimated.[15,16,18] Thus, such an approach suffers from a degree of arbitrariness. As indicated above, here we use the PBE functional only for geometry optimization, and not for electronic structure calculations. To test whether a PBE+U approach could yield noticeably different geometry optimizations, we considered the case of the Cu at In antisite defect, and compared the results obtained with PBE and with the PBE+U set-
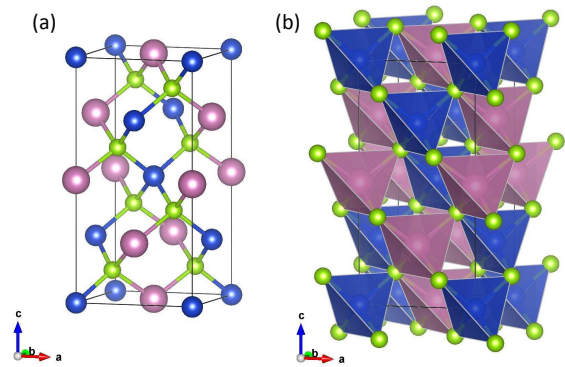

FIG. 1: (a) CuInSe$_2$ conventional tetragonal cell. Blue, pink, and green indicate the Cu, In, and Se atoms, respectively. Each cation is tetrahedrally coordinated by four Se atoms. (b) Plot of the conventional tetragonal cell explicitly showing the Se tetrahedra surrounding the cations. The Se-(112) planes are those facing the origin of coordinates in the plot.

tings of Yamaguchi *et al.* (namely, $U - J = 5$ eV).[30] We found that the preferred location of the antisite is the same in both approaches. Also, the corresponding relaxed ionic coordinates differ in absolute value by only 0.008 Å on average. This results in negligible difference in the quantities of interest in this study, such as hybrid functional total energies and formation energies, including the alignment of reference potentials in the case of charged defects (see Subsection 2.2 further down).

For the electronic properties calculations of the pure and defect supercells we used the HSE hybrid functional,[35] with an amount $\alpha = 0.287$ of exact Hartree-Fock exchange. As we showed before,[26] with this value the HSE hybrid functional reproduces the the experimental band gap of CIS. Furthermore, the main peaks in the electronic density of states (DOS) thus calculated are in very close agreement with those observed in X-ray photoelectron spectroscopy.[36] The DOS and projected density of states (PDOS) were calculated using the tetrahedron method as implemented in VASP.

B. Defect formation energies and transition levels

The formation energy of a defect D, in charge state q, in a bulk compound is given by[31]

$$
\begin{aligned}
E_f[D^q] =& E[D^q] - E[\text{pure}] + \sum_i n_i \mu_i \\
& + q[E_v + E_F + \Delta V] + E_{\text{corr}}(q).
\end{aligned}
\tag{1}
$$

In the above, $E[D^q]$ is the total energy of a supercell containing the defect and $E[\text{pure}]$ is the total energy of the defect-free system. n_i indicates the number of atoms of type i added ($n_i < 0$) or removed ($n_i > 0$) from the supercell, with μ_i the corresponding chemical potential. The chemical potentials depend on the experimental

growth conditions. Their values are very important, as they can have a strong impact on the value of the formation energies and on the predominance of one type of defect or impurity over another at a given E_F. Thermodynamic equilibrium imposes some limiting values to the chemical potentials. Indeed, precipitation of the elemental phases should be avoided, as well as precipitation of competing phases, such as Cu_2Se or $CuIn_5Se_8$. Here, we take the the range of chemical potentials determined in Ref. 26, which considers various possible competing phases.

For charged defects, the chemical potential of the electronic reservoir (Fermi energy) is written $E_v + E_F$, where E_v is the valence band maximum (VBM) of the undoped system. E_F varies, thus, between zero and the gap value. ΔV serves the purpose of aligning the reference (electrostatic) potentials in the doped and undoped systems.[31,37] We calculate ΔV following the procedure introduced in Ref. 38.[39] The last term, $E_{corr}(q)$, is required to correct the total energy from the spurious long-range Coulomb interaction between the defect charge, its periodic images, and the compensating background charge. Here we use[40,41]

$$E_{corr}(q) = -\frac{q^2}{2}\left[\sum_{\mathbf{R}\neq 0}\frac{1}{|\bar{\varepsilon}|}\frac{\mathrm{erfc}(\gamma\sqrt{\mathbf{R}\cdot\bar{\varepsilon}^{-1}\mathbf{R}})}{\sqrt{\mathbf{R}\cdot\bar{\varepsilon}^{-1}\mathbf{R}}} - \frac{\pi}{\Omega\gamma^2}\right.$$
$$\left. + \sum_{\mathbf{G}\neq 0}\frac{4\pi}{\Omega}\frac{\exp(-\mathbf{G}\cdot\bar{\varepsilon}\mathbf{G}/4\gamma^2)}{\mathbf{G}\cdot\bar{\varepsilon}\mathbf{G}} - \frac{2\gamma}{\sqrt{\pi|\bar{\varepsilon}|}}\right]. \tag{2}$$

The sums run over all direct (reciprocal) non-zero $\mathbf{R}$ ($\mathbf{G}$) lattice vectors, $\bar{\varepsilon}$ is the CIS dielectric tensor (| | denotes the determinant), Ω is the volume of the supercell, and γ is a convergence factor.

Of direct experimental interest are the charge transition levels. These determine the preferred charge state of a defect or impurity at a given E_F, and whether it is shallow or deep. Given two possible charge states q and q' for a given defect D, the corresponding charge transition level is[31]

$$\epsilon(q|q') = \left(E_f[D^q]_{E_F=0} - E_f[D^{q'}]_{E_F=0}\right)/(q'-q), \tag{3}$$

where $E_f[D^q]_{E_F=0}$ is the formation energy when the electronic chemical potential is at the VBM.

C. The $\Sigma 3$ grain-boundary model

To put the model in perspective, we recall that CIS has a body-centered tetragonal structure (space group $I\bar{4}2d$, No. 122) with two formula units per unit cell. Fig. 1(a) shows a view of the conventional tetragonal cell. One can see that both cations are tetrahedrally coordinated by four Se atoms, and each Se is coordinated by two Cu and two In atoms. The crystal structure can be seen as
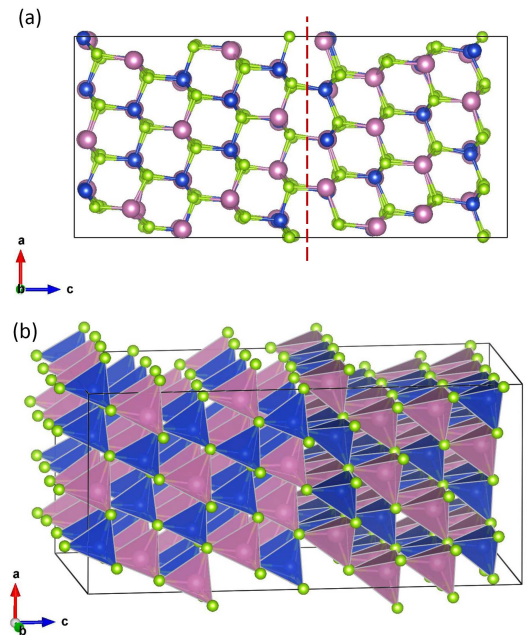

FIG. 2: (a) CuInSe$_2$ $\Sigma 3$ (112) GB 288-atom orthorhombic supercell model. The view is along the b-axis. The dashed line indicates the twin GB plane within the supercell. It is clearly a coherent GB. Because of the periodic boundary conditions, the supercell edges along the c-directions represent an analogous GB plane. (b) The tetrahedra on the right-hand side result from a rotation with respect to the tetrahedra on the left of 60° around the normal to the GB plane.

a distorted zincblende structure, with two cation sublattices instead of only one. The plot of the tetragonal cell in Fig. 1(b) shows that the structure consists of vertex-sharing tetrahedra, with a cation at the center of each tetrahedron and the Se atoms at the vertices.[42]

It has been shown experimentally that among the most common grain boundaries in CIS are $\Sigma 3$ twin grain boundaries along the (112) planes.[43] In Fig. 1(b) the tetrahedra faces turned toward the origin define (112) Se planes. We generated a 288-atom $\Sigma 3$ twin GB supercell model using the GBstudio software,[44] based on a generic diamond structure. The supercell is sufficiently large that it comprises regions with bulk-like behavior.[45] We study here what is known as a cation-Se terminated GB, where the conventional plane separating the two regions with different crystal orientation falls between a cation-(112) surface and a Se-(112) surface.[11] Fig. 2(a) shows a side view of our model supercell, with the c-axis perpendicular to the (112) planes. The conventional GB plane near the middle of the supercell is indicated by a dashed line. Clearly, because of periodicity, the supercell boundaries along the c-axis represent an additional GB plane, similar to the one near the middle. We will refer these as the side and central GBs, respectively. As there are no dislocations or dangling bonds at the boundaries, these are known as coherent GBs.[28]
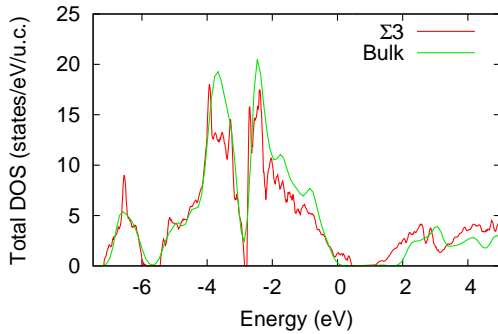
FIG. 3: Comparison of the DOS of bulk CuInSe$_2$ and of the $\Sigma 3$ (112) GB model. They are aligned so that the Cu 3d–Se 4p twin peaks and zero density in between coincide. The two curves are very close to each other, except in the gap region, where the $\Sigma 3$ VBM appears to be higher than in the bulk case, and the CBM appears to be lower. Energy is given with respect to the bulk VBM.

The tetrahedra in Fig. 2(b) illustrate more clearly the nature of the GB. While the tetrahedra on the right side of the GB present a face in the upward direction (i.e., with respect to the a-axis), the tetrahedra on the left present instead an edge. In fact, the right side can be obtained by a rotation arout the c-axis of nearly 60° with respect to the left side.[46] This is typical of twin GBs in cubic systems, i.e., the lattices on both sides of the GB are related by a rotation operation. We note, however, that the periodicity of the CIS structure along the (112) planes is not invariant under a 60° rotation (see Supplementary Information†). The rotation of the lattice on one side of the supercell with respect to the other means that it is not possible for the supercell to preserve the original (112) periodicity on both sides of the GB simultaneously. The periodicity of the supercell replaces it, either on one side of the GB or on both, depending on the specific directions of the a and b axes in the (112) plane. Here, the original periodicity is replaced in the direction of the a-axis on both sides of the GB. We come back to this point in the next Section. Finally, we note that the tetrahedra in Fig. 2(b) show that in the present type of GB the actual planes delimiting the two regions with different lattice orientation are given more precisely by the Se (112) planes next to the conventional GB planes.

III. RESULTS

A. $\Sigma 3$ GB properties

1. Structural aspects

In the present case, the overall stoichiometry of the system is preserved, as well as the tetragonal coordination of the Se atoms at the GBs. Nevertheless, the $\Sigma 3$ structure is of great consequence for the latter. Indeed,

as mentioned earlier, in bulk CIS the Se atoms have a (2 Cu, 2 In) coordination, i.e., they are coordintated by two Cu and two In atoms. However, because of the rotation originating the GB, some of the Se at the GBs see Cu atoms ending up at the position of an In atom, and vice versa, forming antisite pairs. Clearly, such antisite pairs result in Se atoms with anomalous coordination. Specifically, out of the 32 Se atoms at the GBs, eight of them have a (3 Cu, 1 In) coordination, and another eight have a (1 Cu, 3 In) coordination. In addition, one has a (4 Cu, 0 In) coordination, and another one a (0 Cu, 4 In) coordination. Thus, the octet rule is violated by these antisites. At an In$_{Cu}$ antisite there is an excess charge, while at a Cu$_{In}$ antisite there is a lack of charge. The former will tend to donate two electrons, while the latter will tend to accept two electrons (In$_{Cu}^{\bullet\bullet}$ and Cu$_{In}''$, respectively, in the Kröger-Vink notation). Since the antisites occur in pairs, the local neutrality is preserved. As we indicated above, moreover, the original CIS periodicity along the (112) planes is altered. Specifically, a Se atom close to a supercell face along the a-direction will see a Cu atom instead of a In atom as its neighbor in the adjacent supercell, or vice versa. Thus, the octet rule is violated by antisite pairs near these supercell faces as well. Of course, as at the GBs, stoichiometry and local charge neutrality are preserved. We note that In$_{Cu}$-Cu$_{In}$ antisite pairs have long been shown to have a low formation energy in CIS and explain its tendency to disorder.[22] Still, to determine whether our $\Sigma 3$ GB system is stable, or likely to form, we calculate the GB energy,

$$\gamma = \frac{1}{2A}(E_{\text{tot}}[\text{GB}] - nE_{\text{tot}}[\text{bulk}]), \qquad (4)$$

where n is (the equivalent) number of bulk unit cells contained in the GB supercell and A is the GB area.[47] Our HSE calculation yields $\gamma = 0.42$ J/m^2. This is lower than the observed $\Sigma 3$ (111) GB in SrTiO$_3$, i.e., $\gamma = 0.52$ J/m^2, which is considered low.[48] It is also lower than the energy of several types of GBs in ZnO, which have γ values above 1 J/m^2.[47] Thus, we conclude that the GBs we consider here are indeed likely to be present in polycrystalline CIS.

The octet rule violation was first investigated in CIS GBs by Yamaguchi et al.[30] In this interesting study, also based on HSE calculations, the authors show that the octet rule violation can result in a potential barrier at the GB, in addition to affecting the band gap. Here we show that the cation antisites have effects with further, profound consequences. Indeed, below we will see that they have a major effect on defect formation energies, and thus on the relative defect concentrations and ultimately on the electronic character of the GBs.

2. $\Sigma 3$ GB: electronic properties

The electronic structure of the $\Sigma 3$ GB presents some significant differences with the electronic structure of
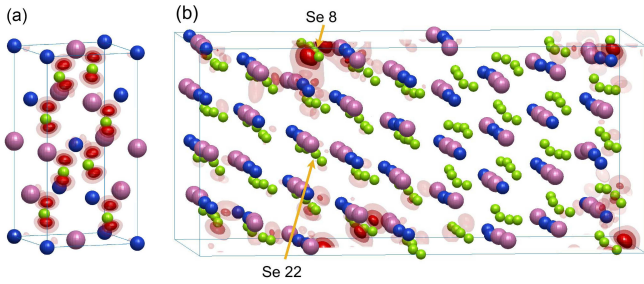
FIG. 4: (a) Probability density isosurfaces, in dark red, medium red, and light red, of the VBM state in the tetragonal unit cell of bulk CuInSe$_2$ (for clarity, the bonds between cations and anions are not depicted). The total probability of finding an electron in the VBM state within the volume enclosed by the dark red isosurface is 1/8. The corresponding probability is 1/4 for the medium red isosurface, and 1/2 for the light red isosurface. The probability density is equally distributed among all Se atoms, i.e., the state is delocalized. The isosurfaces also clearly reveal the predominant Se $4p$ character of the VBM state. (b) Similar plot for the VBM state in the $\Sigma 3$ GB supercell. It has a predominant Se $4p$ character as well, but in this case the probability density is highly localized around specific Se atoms, among which Se atom 8 (see main text). Se atom 22 is also indicated for further reference.

FIG. 5: Comparison of the p- and d-PDOS of a bulk CIS Se atom and of Se atoms 22 and 8 in our GB model. The energy reference is set to the bulk VBM. The plots in (a) and (b) show that Se atom 22 has essentially bulk electronic properties. In contrast, in (c), the p-PDOS of Se atom 8 presents a dramatic increase in a narrow energy range, above the bulk VBM, raising the GB VBM and effectively narrowing its band gap. In (d), the d-PDOS of Se atom 8 shows a similar, although much weaker, effect.

bulk CIS, but also some similarities. The latter has a HSE band gap value of 0.98 eV, calculated as indicated above. It is a direct gap semiconductor, with both the VBM and CBM situated at the Γ point. The GB supercell, on the other hand, has a gap of only 0.11 eV, with the VBM at $\mathbf{k}=(0.5\ 0\ 0)$ in units of the reciprocal vector, and the CBM at the Γ point. We note, however, that the energy of the highest occupied state at Γ is very close to the VBM value, the difference being of only $\sim$13 meV. In Fig. 3 we align the bulk and the $\Sigma 3$ GB DOS, matching the well-known Cu $3d$-Se $4p$ twin peaks in the valence band (we set the VBM of bulk CIS to 0).[3,26] Apart from the clear band gap narrowing, the plot demonstrates great similarity between the DOS of the two systems. The alignment also suggests that the band gap narrowing in the $\Sigma 3$ GB electronic structure obeys to both a raising of the VBM and a lowering of the CBM.[49]

To shed light on what causes this, we compare the VBM and CBM states of both systems. In Figs. 4(a) and (b) we plot probability density isosurfaces of the VBM state in the bulk and GB systems, respectively.[50] In each case, three isosurfaces are shown, as detailed in the figure caption. In Fig. 4(a), it is interesting to see that although the upper valence bands in CIS arise largely from hybridized Cu $3d$-Se $4p$ states, the VBM probability density is higher around the Se atoms, revealing a predominant Se $4p$ character. Further, the probability density is equally distributed among all Se atoms, i.e., the the VBM state is delocalized. Fig. 4(b) shows that in the GB the VBM keeps its predominant Se $4p$ character, but is highly localized around specific Se atoms,
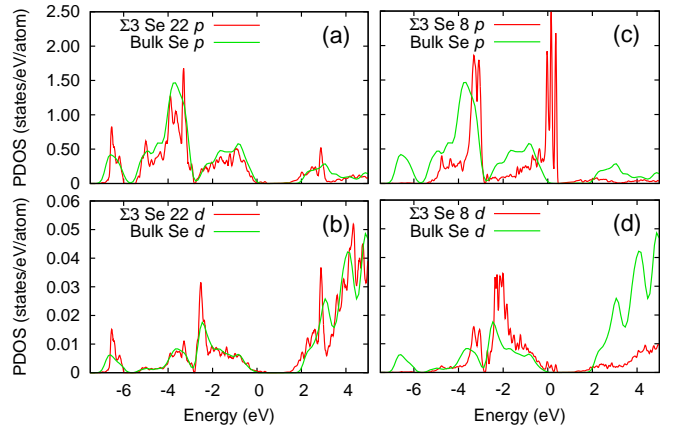
in stark contrast with the bulk. Closer inspection of the atomic structure in the vicinity of the three Se atoms with higher probability densities reveals that two of them have a (4 Cu, 0 In) coordination [Se atom 8 and Se atom at the top right in Fig. 4(b)], and the third one a (3 Cu, 1 In) coordination.[51] The reason for the higher probability density at those locations is thus clear. Indeed, it is well known that Se p-Cu d hybridization in the ternary chalcogenides has a strong influence on the VBM, tending to push it upward compared to compounds with other transition metals with more localized d orbitals (such as Zn or Cd in ZnSe and CdSe).[20] Thus, the stronger p-d repulsion at the location of the mentioned Se atoms pushes locally upward the highest occupied levels compared to locations where the Se atoms conserve the normal coordination.

To corroborate this interpretation, we compare the local PDOS of one of the Se atoms coordinated by four Cu atoms (Se atom 8), and of a Se atom coordinated normally, away from the GBs and edges of the supercell [Se atom 22 in Fig. 4(b)], which can be expected to have a more bulk-like PDOS. In Figs. 5(a) and 5(b) we first compare the p and d PDOS of Se atom 22 with the corresponding PDOS of a bulk Se atom (as for Fig. 3, the bulk CIS VBM is taken as energy reference). The curves were again aligned so that the Cu $3d$-Se $4p$ key features coincide. The plot shows a remarkable similarity between the two curves, demonstrating essentially similar electronic properties. In contrast, Figs. 5(b) and 5(d) show that Se atom 8 presents very different PDOS curves. Indeed, there is a dramatic increase of the p character PDOS just below the $\Sigma 3$ supercell VBM, where the Se atom 22 and
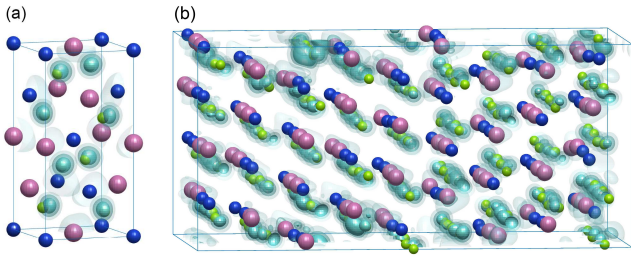
FIG. 6: Probability density isosurfaces, in dark cyan, medium cyan, and light cyan, of the CBM state in (a) bulk $CuInSe_2$2 and (b) the $\Sigma3$ GB supercell. Similar to Fig. 4, the total probabilities of finding an electron within the three isosurfaces mentioned are 1/8, 1/4, and 1/2, respectively. Both in the bulk and in the GB supercell the CBM state is predominantly of Se $4sp$ character and is clearly delocalized (albeit the fact that the probability is not as uniformly distributed in the case of the GB supercell).

the bulk Se atoms have both a negligible PDOS. In the case of the d character PDOS, it is also higher in Se atom 8, although the difference is not so large. This confirms that the band gap narrowing is in part due to a raising of the VBM. It is important to note that this is a local effect, due to the presence of Se atoms with higher Cu coordination.

An analysis of the PDOS also indicates that, notably, the CBM lowering is not a local effect, i.e., it is present for all atoms. Indeed, this is seen in all four cases in Fig. 5. This conclusion is corroborated by a plot of the probability density of the CBM state. This is shown in Fig. 6, where we compare the CBM probability densities of bulk $CuInSe_2$ and the $\Sigma3$ supercell. In both cases, the probability density is delocalized. Albeit the fact that in the $\Sigma3$ supercell the probability is high in a larger volume around the high Cu coordination Se atoms, it reaches equally high values around all the other Se atoms. The plots also illustrate the predominant Se $4sp$ character of the CBM state. We note that the delocalization of the CBM state implies that the GBs (or the antisite pairs at the edges of the supercell) will not result in a significant localization of shallow donor levels in the supercell. This is relevant because type inversion is often observed at GBs (i.e., from p-type in the grains to n-type at the GBs), implying reduced GB recombination and enhanced carrier collection.[6] Thus, it is important that there is no carrier localization near the GBs.

B. Defects at the GB

The defects we study here are the point defects Cu vacancy (V_{Cu}), In at Cu (In_{Cu}), Cu at In (Cu_{In}), and Na at Cu (Na_{Cu}), as well as the $2V_{Cu} + In_{Cu}$ complex at the GB interface. The importance of these defects has been already pointed out in previous works.[22,26,52] Be-
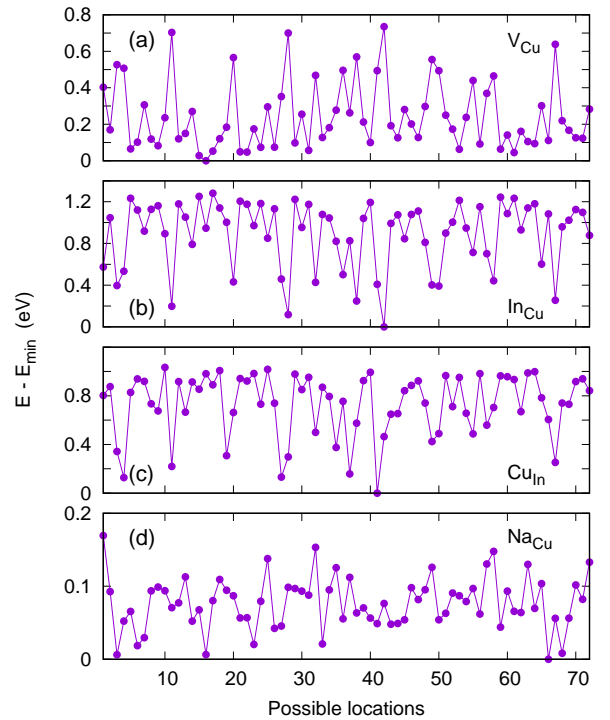

FIG. 7: Plot of the total energies of the defect-containing $\Sigma3$ GB supercells $vs.$ position of the defect, for all four point defects considered in this study.

cause of the broken symmetry due to the GBs and the antisite defects, the 72 Cu atoms in the supercell (as well as the 72 In atoms) are inequivalent. Thus, to find the preferred location for the above point defects, we performed a geometry optimization, as indicated in Subsection II A, for each of the 72 possible positions. In the case of the complex, we placed it directly at the central GB, adopting the (112) geometry determined by Zhang and co-workers[22] and also relaxed the structure. In Fig. 7 we plot the total energies $vs.$ possible positions for all four point defects considered (the numbering of the Cu atoms is arbitrary, but fixed).

We also calculated the formation energies for all the above defects, both in In-rich and In-poor growth conditions. As already mentioned, for this we use the chemical potentials determined in Ref. 26. For the image-charge correction [see Eq. (2)], we took the experimental dielectric tensor values, i.e., $\epsilon_\perp = 25.5$ and $\epsilon_\parallel = 23.7$.[53] Because of the different crystal orientations present in our GB model, for the calculations we used the average value $\epsilon_{av} = (2\epsilon_\perp + \epsilon_\parallel)/3$, similar to what is done for polycrystalline materials.[54] The image-charge corrections to the formation energies are small, however, due to the rather large dielectric tensor components. In Fig. 8 we plot the formation energies for the two growth conditions mentioned. For completeness and for the discussions further on, we also plot the formation energies for bulk CIS. In-rich growth conditions used correspond to n-type CIS,
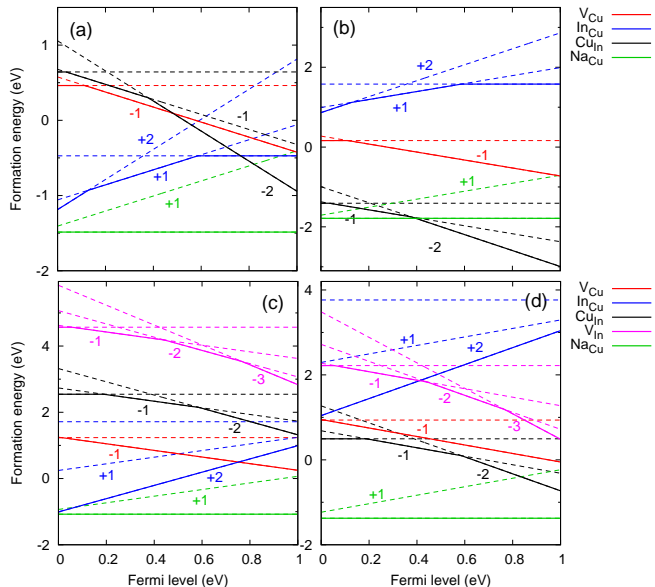
FIG. 8: Neutral and charged defect formation energies as a function of Fermi level in the CIS $\Sigma 3$ supercell [(a) and (b)] and in bulk CIS [(c) and (d)]. Figures (a) and (c) correspond to In-rich growth conditions and figures (b) and (d) to In-poor conditions. The continuous solid lines indicate the preferred charge state as a function of Fermi level energy.

while the In-poor growth conditions correspond to p-tpye CIS.[26] The preferred charge state as a function of Fermi level is indicated in Fig. 8 by the solid lines. The dotted lines show the formation energy of the different charge states in the full Fermi level range (see Supplementary Information† for more details on the formation energies). We note that the formation energies in Ref. 26 are somewhat different from those in Figs. 8(c) and (d). This is because in that reference the incorrect ΔV sign was used, and the image charge corrections were not taken into account. However, the differences are mainly quantitative, and the conclusions there reported remain essentially valid.

In the following, we discuss the structural aspects of the native point defects. Their electronic properties and effects are discussed in Subsection III C. Although we cannot address directly electrical transport, we will see that our calculations provide important qualitative information about the influence of the defects considered on carrier concentration, carrier type, and the possible creation of potential barriers, allowing us to discuss their effects on the electrical and carrier transport properties of the GBs.

1. V_{Cu}

An analysis of the results in Fig. 7(a) reveals that the cost of creating a vacancy at the location of a Cu atom

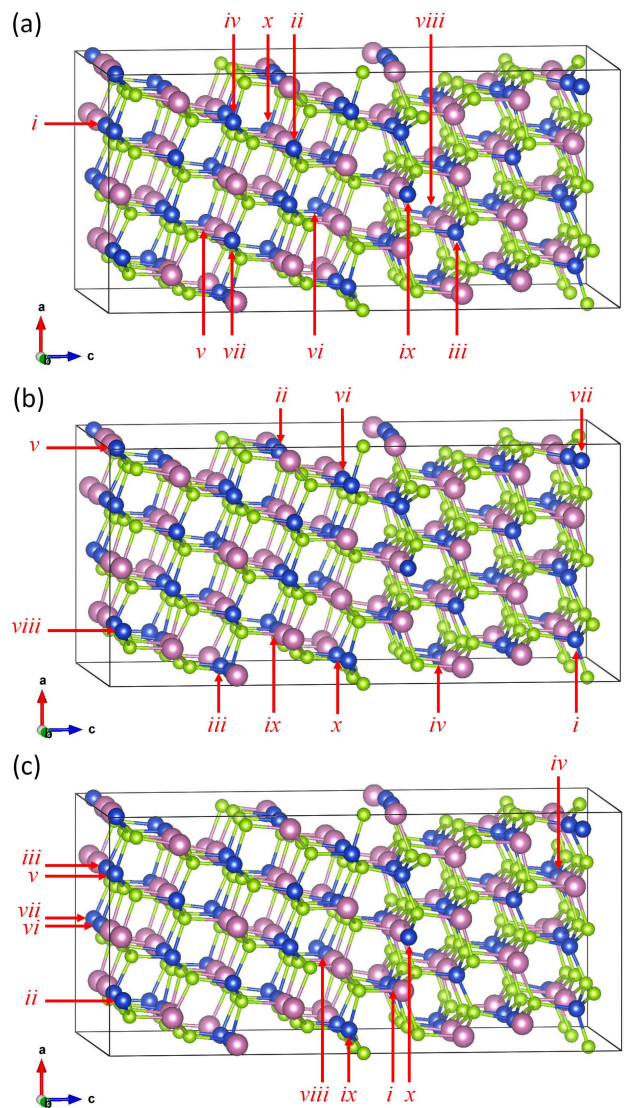FIG. 9: Location of the ten lowest energy positions for (a) V_{Cu}, (b) In_{Cu}, and (c) Na_{Cu}. The numbering is such that $E_i < E_{ii} \ldots < E_x$. (a) The V_{Cu} with the lowest energy (i) is at the side GB, but the other nine lowest energy locations occur throughout the supercell. (b) The ten In_{Cu} lowest energy locations occur at the GBs or supercell edges. (c) All ten Na_{Cu} lowest energy locations are at the GBs. See Supplementary Information† for an illustration of the GBs with the defects at their lowest energy locations.

greatly depends on the coordination of the four Se atoms it is bound to. Indeed, the V_{Cu} locations with highest energies correspond systematically to Cu bound to either a (3 Cu, 1 In) or (4 Cu, 0 In) coordinated Se atom. Thus, a V_{Cu} is more likely to be formed around a normally coordinated Se atom. However, these occur both at the GBs and away from them. In Fig. 9(a) we indicate with an arrow the locations corresponding to the ten lowest V_{Cu} energy positions. As can be seen, the lowest energy location (i) is at a side GB. A calculation of the formation en-

ergy of V_{Cu} (in the neutral state) in that position shows that it is 0.77 eV lower than in the bulk (see Fig. 8).[55] This clearly indicates that V_{Cu} is more likely to form at the GB. In p-type conditions, a sufficiently low Cu chemical potential (e.g., $\Delta\mu_{Cu} = -0.75$ eV; see Ref. 26) can result in a decrease in Cu concentration at the GB, as observed in experiment.[11] However, in less favorable growth conditions the concentration of Cu vacancies at the GB and in the bulk would be small, implying that any difference in Cu concentration would be difficult to observe. Moreover, the second lowest energy location for V_{Cu} in the supercell, which is one atomic layer removed from the central GB [location ii in Fig. 9(a)], has an energy only 28 meV higher than location i. In fact, the energy difference between the lowest and tenth lowest energy locations indicated in Fig. 9(a) is 65 meV. This means that temperature effects may dampen the preference of V_{Cu} to form at the GB (growth temperatures between 400 °C and 600 °C are typical[4]). This is more in line with the results of Yan and co-workers, who did not find a significant Cu deficiency at a cation-Se $\Sigma3$ GB.[7] Thus, our results indicate that work under different growth conditions can be at the origin of the seemingly contradicting results reported by different groups.

2. In_{Cu}

A comparison of Figs. 7(a) and (b) immediately reveals a striking anticorrelation between the preferred locations for In_{Cu} and V_{Cu}. Where the formation energy of In_{Cu} is lowest, the formation energy of V_{Cu} is highest, and vice versa. Thus, In substitutes preferentially Cu atoms bound to a (4 Cu, 0 In) or (3 Cu, 1 In) coordinated Se atom (where V_{Cu} is least likely to form, as discussed above). So the subsitution tends to restore the octet rule. The ten locations with lowest In_{Cu} formation energy are indicated with an arrow in Fig. 9(b). It is not surprising that these locations fall at the GBs and close to the supercell faces along a-axis direction, as there is where the anomalous coordination occurs. As for V_{Cu}, the lowest energy location is at the side GB. But compared to the V_{Cu} case, the the energy difference between location i and the other locations is much larger. Indeed, the energy difference between locations ii and i is 118 meV (compared to 28 meV in the case of V_{Cu}). Thus, the tendency to form at the GB is stronger. The comparison with the formation energy in the bulk is more conclusive, as we find that the formation energy of In_{Cu} in the bulk is 2.19 eV higher than at the GB (see Fig. 8). This should result in substantial In enrichment and Cu depletion at the GB. This has been observed experimentally,[9,11,12] especially at non-$\Sigma3$ GBs. On the other hand, in Ref. 11 Cu depletion but no In enrichment was observed at a cation-Se terminated (112) $\Sigma3$ GB. We discuss further this point below, in connection with the Cu_{In} antisites defects.

3. Cu_{In}

The analysis of the locations of the In atoms for which the energy of Cu_{In} is lowest shows that Cu substitutes preferentially In atoms bound to anomalously coordinated Se atoms, i.e., either (1 Cu, 3 In) or (0 Cu, 4 In). Furthermore, on close inspection we find the In atoms preferentially substituted are immediate neighbors of the Cu atoms at which the energy of In_{Cu} is lowest. This is quite understandable, because an antisite pair giving rise to (3 Cu, 1 In) coordinated Se atoms, also gives rise to (1 Cu, 3 In) coordinated Se atoms in its immediate neighborhood. This is the reason for the strong correlation between the results in Figs. 7(b) and (c). Just as In_{Cu} defects, Cu_{In} defects will occur mostly at the GBs. Fig. 8 shows that in In-poor conditions the formation energy of Cu_{In} is lower than the formation energy of In_{Cu}, while it is the reverse in In-rich conditions. The formation energy of V_{Cu} also changes importantly. Actually, the relatively narrow range of Cu chemical potentials for which CIS is stable[26,52] implies that the chemical potential of In plays a major role in determining the formation energies of these defects. There is an apparent trade-off between these as a function of In chemical potential. This can explain the observed Cu depletion with no In enrichment at the cation-Se GBs in Ref. 11. Indeed, in a certain In chemical potential range, Cu_{In} and In_{Cu} will tend to compensate, resulting in Cu depletion alone due to V_{Cu}.

4. Na_{Cu}

The beneficial effects of Na on the performance of CIGS photovoltaic cells have been extensively discussed.[1,6,56,57] It has also been reported that it segregates to the GBs, where if forms Na_{Cu} defects,[9,58] but this has not been addressed theoretically previously.

The range of energies for Na_{Cu} in Fig. 7(d) is narrower than for the other defects (four to seven times narrower). Thus, the energy difference between the lowest energy locations for Na_{Cu} can be expected to be rather small. For instance, the difference in energy between the lowest and second lowest energy locations is 6 meV (compared to 118 meV and 128 meV for In_{Cu} and Cu_{In}, respectively). What is more, the energy difference between the lowest and tenth lowest energy locations is 44 meV. Remarkably, as shown in Fig. 9(c), all these locations fall at the $\Sigma3$ GBs. In fact, of the 20 locations with the lowest energies, only three are not at one of the GBs. This clear tendency to form at the GBs is corroborated by a direct comparison of the formation energy of Na_{Cu} at the GB and in the bulk. In the latter case the energy is 0.41 eV higher. We note that the Na_{Cu} formation energies in Fig. 8 correspond to Na-rich conditions, i.e., the Na chemical potential is obtained from the energy of Na in its metallic phase ($\mu_{Na} \simeq -1.4$ eV). Clearly, there can be an important concentration of Na_{Cu} defects

even in relatively Na-poor conditions. Our results are in complete agreement with the experimental findings mentioned above.

5. $2V_{Cu}$-In_{Cu}

The $2V_{Cu}$-In_{Cu} complex has been found to have a low formation energy in the bulk.[22,52] It was also proposed to be at the origin of the Cu depletion at CIS GBs discussed above.[13,52] These complexes were calculated to form on (112) planes in CIS, where the two vacancies are fcc nearest neighbors to In_{Cu} and third fcc nearest neighbors of each other (see Ref. 22). Thus, we located with that geometry the $2V_{Cu}$-In_{Cu} complex at the central GB. The formation energy in the two growth conditions considered in this study are very high, as can be seen in Figs. 8. In extreme Cu-poor conditions its formation energy can be very low (not shown here). But the interest of Cu-poor conditions is academic to some extent, as the limited range of Cu chemical potentials values for which CIS is stable falls toward the Cu-rich end.[26,52]

The reason for the high formation energy in the present case can be understood as follows. As discussed above, the formation energy of V_{Cu} is low around normally coordinated Se atoms, while In_{Cu} has a low formation energy around (3 Cu, 1 In) and (4 Cu, 0 In) coordinated Se atoms. However, the vacancies and antisite in the $2V_{Cu}$-In_{Cu} complexes with the above mentioned geometry that can be accomodated in our GBs do not fall in those categories. Thus, this complex is unlikely to lead to Cu depletion in the present type of $\Sigma 3$ GB.

C. Effect of the defects on the electronic properties of the GB

We first discuss the electrical nature of the defects in Fig. 8. In the bulk, V_{Cu} is known to act as a shallow acceptor,[22,26,52] as Figs. 8(c) and (d) also show. At the GB, the $\epsilon(-|0)$ transition level is finite, with a value of 115 meV above the VBM. This can still be considered a relatively shallow acceptor.[22] As in the bulk, it is the main acceptor in In-rich conditions, but loses its predominance in In-poor conditions. In the case of In_{Cu}, we find an important difference with respect to the bulk. In the latter case, In_{Cu} is a shallow donor in the +2 charge state, while at our GB it is a deep donor, with a $\epsilon(+|0)$ transition level at ~ 0.41 eV below the CBM. Conversely, Cu_{In} is a very shallow acceptor in the -1 charge state at the GB ($\epsilon(0|-)$ transition level 35 meV above the CBM), while it is somewhat deep in the bulk, with a $\epsilon(-|0)$ transition level at 190 meV above the VBM (this is close to what is found in Ref. 52 and much lower than the value of 290 meV reported in Ref. 22). Finally, Na_{Cu} is expected to be mainly in its neutral state.[3] This is what we find, both in the bulk and at the GB, as shown in Fig. 8.
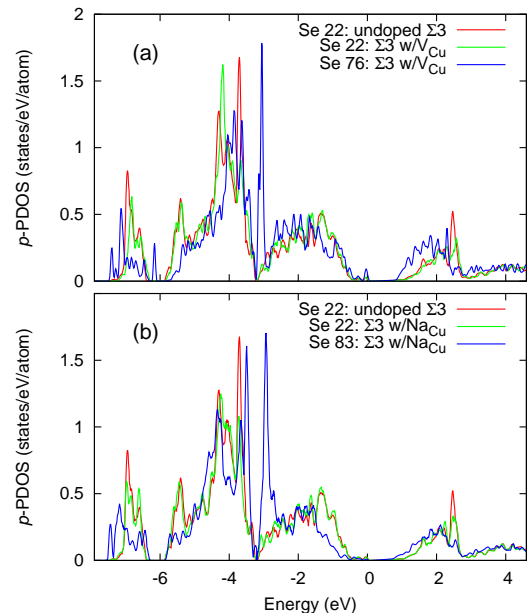
As already mentioned, in Ref. 26 it was shown that

FIG. 10: (a) Comparison of the p-PDOS of Se atom 22 in the undoped $\Sigma 3$ supercell and Se atoms 22 and 76 (nearest neighbor to V_{Cu}) in the $\Sigma 3$ supercell with V_{Cu}. (b) Comparison of the p-PDOS of Se atom 22 in the undoped $\Sigma 3$ supercell and Se atoms 22 and 83 (nearest neighbor to Na_{Cu}) in the $\Sigma 3$ supercell with Na_{Cu} (energies referenced to the $\Sigma 3$ VBM).

CIS is n-type when grown in In-rich conditions, while it is p-type if grown in In-poor conditions. This can be deduced from Figs. 8(c) and (d) as well (recall that the Fermi level is determined mainly by the lowest formation energy charged defects). At the GBs, the Na_{Cu} appears to play a very important role. In In-poor conditions, without Na defects the GB would be p-type because of the Cu_{In} defects. This would be detrimental to cell efficiency, as the GB would tend to be hole-rich and result in carrier recombination. But, as can be seen in Fig. 8(b), in those conditions Na_{Cu} will tend to passivate those defects. This is in agreement with the observation that Na is beneficial to the performance of the CIGS PV cells. Furthermore, in In-rich conditions, as can be deduced from Fig. 8(a), without Na defects the self-consistent Fermi level will fall toward the center of the gap, far from the VBM and CBM, resulting in depletion of carriers. But Na_{Cu} defects push the Fermi level toward the CBM, i.e., the GB will tend to be n-type. This coincides with the observation that carrier depletion and even type inversion occurs in CIGS GBs[6,8] Our finding, thus, provides a possible mechanism for this.

Also of interest is the role of V_{Cu} and Na_{Cu} regarding carrier transport. Indeed, since the seminal work of Persson and Zunger,[13] the idea that the mentioned defects could give rise to hole barriers at the GBs has often been discussed.[6,7,9] The reasoning is that both V_{Cu} and Na_{Cu} result in a local lack of d-electrons, and thus the absence of p-d repulsion can results in a local lowering of

the VBM, thus creating a barrier to hole transport. In Fig. 10(a), we compare the p-PDOS of three Se atoms. Se atom 22 in our GB supercell was shown above to have a bulk-like PDOS. We can see in the figure that the same atom in the GB supercell with V_{Cu} has a very similar PDOS. This indicates that it is very little affected by the vacancy. We further considered the p-PDOS of the four Se atoms directly neighboring V_{Cu}. One of these atoms is Se atom 76 (see Supplementary Information†), and we also plot its p-PDOS in the figure. As can be seen, the effect on the position of the local VBM is rather weak. The effect is stronger at higher binding energies and at the CBM, but this will not result in a hole barrier. The effect on the VBM of remaining the Se atoms is even weaker.

The case of Na_{Cu}, in Fig. 10(b), is somewhat different. There again the difference between the p-PDOS of Se atom 22 in the GB supercell with and without the defect is negligible, indicating in the latter case Se atom 22 remains bulk-like. In contrast, Se atom 83, which is one of the nearest neighbors of Na_{Cu} (see Supplementary Information†), clearly shows a strongly reduced p-PDOS at the VBM onset compared to Se atom 22. Although the other three Se atoms surrounding Na_{Cu} are much less affected (not shown), the effect on Se atom 83 cannot be ignored. We conclude, thus, that while the effect of V_{Cu} on the local VBM is very weak and is not likely to have a strong effect on transport, Na_{Cu} does seem capable of producing a hole barrier at the GB if present in sufficient quantities. This is plausible because, as we indicated, it is known to accumulate at the GBs.[9,57] (In the Supplementary Information† we also briefly discuss the role of the possible formation of $NaInSe_2$ at the GB.)

IV. SUMMARY AND CONCLUSIONS

We use advanced first-principles methods to study a model of a coherent $\Sigma 3$ (112), cation-Se terminated GB. Because of its simplicity (i.e., it does not present dangling bonds nor any strong reconstruction), such a GB has been assumed to have mild overall effects on the properties of polycrystalline CIS.[12,18] We show here, however, that in spite of its apparent simplicity, this GB can have strong influence on the properties of the latter. This is to a large extent due to the antisite cation pairs that are formed at the GB.

We have shown that the defect formation energies and transition levels are different from those in the bulk. We have shown that the competing concentrations of V_{Cu}, In_{Cu}, and Cu_{In} can explain the Cu depletion without In enrichment observed in cation-Se GBs. Regarding electrical properties, we found that Na_{Cu} forms easily at the GBs and provides a mechanism for the carrier depletion (in In-poor conditions) and even type inversion (in In-rich conditions) experimentally observed at GBs, both of which lead to spatial separation between photogenerated electrons and holes, thus reducing carrier recombination. Moreover, it can passivate holes at the GB, which can explain the beneficial effects of Na on the efficiency of CIGS PV cells. In addition, Na_{Cu} is capable of producing an efficient hole barrier at the GB. On the other hand, we also found that although V_{Cu} will tend to form at the GBs, its effect as hole barrier will be very weak.

There are many types of GBs possible in CIS (and, more generally, in CIGS), and it is not possible to consider all of them in a single study. Further research will be necessary to achieve a deeper understanding of their properties and effect on cell efficiency. The present study suggests a path for future work.

Acknowledgements

[1] P. Jackson, R. Wuerz, D. Hariskos, E. Lotter, W. Witte, and M. Powalla, Phys. Status Solidi RRL **10**, 583 (2016).

[2] www.nrel.gov/pv/assets/images/efficiency-chart.png

[3] S. Siebentritt, M. Igalson, C. Persson, and S. Lany, Prog. Photovolt: Res. Appl. **18**, 390 (2010).

[4] M. Theelen and F. Daume, Solar Energy **133**, 586 (2016).

[5] S. R. Thomas, C.-W. Chen, M. Date, Y.-C. Wang, H.-W. Tsai, Z. M. Wang, and Y.-L. Chueh, RSC Advances **6**, 60643 (2016).

[6] U. Rau, K. Taretto, and S. Siebentritt, Appl. Phys. A **96**, 221 (2009).

[7] Y. Yan, R. Noufi, and M. M. Al-Jassim, Phys. Rev. Lett. **96**, 205501 (2006).

[8] S. Sadewasser, D. Abou-Ras, D. Azulay, R. Baier, I. Balberg, D. Cahen, S. Cohen, K. Gartsman, K. Ganesan, J. Kavalakkatt, W. Li, O. Millo, Th. Rissom, Y. Rosenwaks, H.-W. Schock, A. Schwarzman, and T. Unold, Thin Solid Films **519**, 7341 (2011).

[9] P.-P. Choi, O. Cojocaru-Mirédin, R. Wuerz, and D. Raabe, J. Appl. Phys. **10**, 124513 (2011).

[10] C.-S. Jiang, M. A. Contreras, I. Repins, H. R. Moutinho, Y. Yan, M. J. Romero, L. M. Mansfield, R. Noufi, and M. M. Al-Jassim, Appl. Phys. Lett. **101**, 033903 (2012).

[11] D. Abou-Ras, B. Schaffer, M. Schaffer, S. S. Schmidt, R. Caballero, and T. Unold, Phys. Rev. Lett. **108**, 075502 (2012).

[12] D. Abou-Ras, S. S. Schmidt, N. Schäfer, J. Kavalakkatt, T. Rissom, T. Unold, R. Mainz, A. Weber, T. Kirchartz,

E. S. Sanli, P. A. van Aken, Q. M. Ramasse, H.-J. Kleebe, D. Azulay, I. Balberg, O. Millo, O. Cojocaru-Mirédin, D. Barragan-Yani, K. Albe, J. Haarstrich, and C. Ronning, Phys. Status Solidi RRL **10**, 363 (2016).

[13] C. Persson and A. Zunger, Phys. Rev. Lett. **91**, 266401 (2003).

[14] Y. Yan, C.-S. Jiang, R. Noufi, S.-H. Wei, H. R. Moutinho, and M. M. Al-Jassim, Phys. Rev. Lett. **99**, 235504 (2007).

[15] W.-J. Yin, Y. Wu, R. Noufi, M. Al-Jassim, and Y. Yan, Appl. Phys. Lett. **102**, 193905 (2013).

[16] Y. Yan, W.-J. Yin, Y. Wu, T. Shi, N. R. Paudel, C. Li, J. Poplawsky, Z. Wang, J. Moseley, H. Guthrey, H. Moutinho, S. J. Pennycook, and M. M. Al-Jassim, J. Appl. Phys. **117**, 112807 (2015).

[17] J. Bekaert, R. Saniz, B. Partoens, and D. Lamoen, J. Appl. Phys. **117**, 015104 (2015).

[18] H. Mirhosseini, J. Kiss, and C. Felser, Phys. Rev. Appl. **4**, 064005 (2015).

[19] T. Tinoco, C. Rincoón, M. Quintero, and G. Sánchez Peŕez, Phys. Status Solidi **124**, 247 (1991).

[20] J. E. Jaffe and A. Zunger, Phys. Rev. B **28**, 5822 (1983).

[21] M. Belhadj, A. Tadjer, B. Abbar, Z. Bousahla, B. Bouhafs, and H. Aourag, Phys. Stat. Sol. (b) **241**, 2516 (2004).

[22] S. B. Zhang, S.-H. Wei, Alex Zunger, and H. Katayama-Yoshida, Phys. Rev. B **57**, 9642 (1998).

[23] C. Domain, S. Laribi, S. Taunier, and J. F. Guillemoles, J. Phys. Chem. Solids **64**, 1657 (2003).

[24] C. Persson, Y.-J. Zhao, S. Lany, and A. Zunger, Phys. Rev. B **72**, 035211 (2005).

[25] J. Pohl and K. Albe, Phys. Rev. B **87**, 245203 (2013).

[26] J. Bekaert, R. Saniz, B. Partoens, and D. Lamoen, Phys. Chem. Chem. Phys. **16**, 22299 (2014).

[27] GBs are the interfaces between crystallites with different lattice orientation. Superimposing the two misoriented lattices may give rise to a lattice of coinciding lattice points, the coincidence site lattice (CSL). A GB is denoted Σn if the ratio between the volumes of the unit cells of the CSL and of the original lattice is n.[6,28] In the present case, we have $n = 3$.

[28] L. Priester, *Grain Boundaries: from theory to engineering* (Springer, Dordrecht, 2013).

[29] H. Yamaguchi and T. Mizoguchi, J. Ceram. Soc. Jpn. **122**, 469 (2014).

[30] H. Yamaguchi, H. Hiramatsu, H. Hosono, and T. Mizoguchi, Appl. Phys. Lett. **104**, 153904 (2014).

[31] C. Freysoldt, B. Grabowski, T. Hickel, J. Neugebauer, G. Kresse, A. Janotti, and C. G. Van de Walle, Rev. Mod. Phys. **86**, 253 (2014).

[32] G. Kresse and J. Furthmüller, Phys. Rev. B **54** , 11169 (1996).

[33] G. Kresse and D. Joubert, Phys. Rev. B **59**, 1758 (1999).

[34] J. P. Perdew, K. Burke, and M. Ernzerhof, Phys. Rev. Lett. **77**, 3865 (1996).

[35] J. Heyd and G. E. Scuseria, J. Chem. Phys. **118**, 8207 (2003); J. Heyd, J. E. Peralta, G. E. Scuseria, and R. L. Martin, *ibid* **123**, 174101 (2005).

[36] T. V. Kuznetsova, V. I. Grebennikov, H. Zhao, C. Derks, C. Taubitz, M. Neumann, C. Persson, M. V. Kuznetsov, I. V. Bodnar, R. W. Martin, and M. V. Yakushev, Appl. Phys. Lett. **101**, 111607 (2012).

[37] T. Mattila and A. Zunger, Phys. Rev. B **58**, 1367 (1998).

[38] R. Saniz, Y. Xu, M. Matsubara, M. N. Amini, H.Dixit, D.Lamoen, and B.Partoens, J. Phys. Chem. Solids **74**, 45 (2013).

[39] We call the attention on the fact that in Ref. 38 the sign of ΔV is incorrect. The correct sign is used here.

[40] G. Petretto and F. Bruneval, Phys. Rev. Appl. **1**, 024005 (2014).

[41] Y. Kumagai and F. Oba, Phys. Rev. B **89**, 195205 (2014).

[42] Crystal structure plots were made using VESTA. See K. Momma and F. Izumi, J. Appl. Crystallogr. **44**, 1272 (2011).

[43] D. Abou-Ras, S. Schorr, and H. W. Schock, J. Appl. Cryst. **40**, 841 (2007).

[44] staff.aist.go.jp/h.ogawa/GBstudio

[45] GBstudio performs purely geometrical operations (no atomic relaxations) on the two misoriented sublattices to obtain a CSL with a unit cell three times larger the than CIS unit cell. The supercell output is the smallest one containing the corresponding GB.

[46] The actual angle is $\sim 61.3°$. The small deviation from $60°$ arises because the cation triangles on the ab-plane are not exactly equilateral. This is due to a a/b ratio slightly away from ideal.

[47] W. Körner, P. D. Bristowe, and C. Elsässer, Phys. Rev. B **84**, 045305 (2011).

[48] S. Hutt, S. Köstlmeier, and C. Elsässer, J. Phys.: Condens. Matter **13**, 3949 (2001).

[49] For all curve plots we use *gnuplot* (gnuplot.sourceforge.net), unless othwerwise specified.

[50] To create the plots in Figs. 4 and 6 we used MATLAB (MATLAB 2016b, The MathWorks, Inc., Natick, Massachusetts, United States).

[51] There is third case of a Se atom coordinated by four Cu atoms, but its contribution is outweighed by the ones mentioned.

[52] S. Chen, A. Walsh, X. G. Gong, and S.-H. Wei, Adv. Mater. **1998**, 1522 (2013).

[53] O. Madelung, *Semiconductors Data Handbook* (Springer, Berlin, 2004).

[54] S. G. Choi, J. Kang, J. Li, H. Haneef, N. J. Podraza, C. Beall, S.-H. Wei, S. T. Christensen, and I. L. Repins, Appl. Phys. Lett. **106**, 043902 (2015).

[55] In Ref. 29 a much smaller energy difference is reported, namely 80 meV. However, the work in that reference is based on the PBE+U functional, casting some doubt on its results. Also, there is a strong discrepancy between the band gap value there reported (which is close to the experimental value) and the much lower values obtained with such a functional in previous and more recent work.[15,18]

[56] L. Kronik, D. Cahen, and H. W. Schock, Adv. Mater. **10**, 31 (1998).

[57] A. Rockett, Thin Solid films **480**, 2 (2005).

[58] C.-S. Jiang, R. Noufi, J. A. AbuShama, K. Ramanathan, H. R. Moutinho, J. Pankow, and M. M. Al-Jassim, Appl. Phys. Lett. **84**, 3477 (2004).